A New Synaptic Plasticity Rule for Networks of Spiking Neurons

Waldemar Swiercz, Krzysztof Cios, *Senior Member, IEEE*, Kevin Staley, Lukasz Kurgan, *Member, IEEE*, Frank Accurso, and Scott Sagel

***Abstract*—In this paper, we describe a new Synaptic Plasticity Activity Rule (SAPR) developed for use in networks of spiking neurons. Such networks can be used for simulations of physiological experiments as well as for other computations like image analysis. Most synaptic plasticity rules use artificially defined functions to modify synaptic connection strengths. In contrast, our rule makes use of the existing postsynaptic potential values to compute the value of adjustment. The network of spiking neurons we consider consists of excitatory and inhibitory neurons. Each neuron is implemented as an integrate-and-fire model that accurately mimics the behavior of biological neurons. To test performance of our new plasticity rule we designed a model of a biologically-inspired signal processing system, and used it for object detection in eye images of diabetic retinopathy patients, and lung images of cystic fibrosis patients. The results show that the network detects the edges of objects within an image, essentially segmenting it. Our ultimate goal, however, is not the development of an image segmentation tool that would be more efficient than nonbiological algorithms, but developing a physiologically correct neural network model that could be applied to a wide range of neurological experiments. We decided to validate the SAPR by using it in a network of spiking neurons for image segmentation because it is easy to visually assess the results. An important thing is that image segmentation is done in an entirely unsupervised way.**

***Index Terms*—Modeling, neural networks, synaptic plasticity.**

I. Introduction

ARTIFICIAL neural networks of spiking neurons (NSN) are used for computer modeling of biological neural circuits and allow for observation of interactions between neurons. They were also used as a data processing tool, e.g., for pixel clustering [40]. Major elements of any NSN are the neuron model, synaptic connections structure (network topology), and synaptic plasticity (the learning rules). It is important for a neuron model to mimic the spiking nature of biological neurons and closely simulate the dynamics of a membrane potential, refractory properties, and adaptation to stimulation. Biological neurons generate a series of action potentials (trains of spikes) in response to stimulation. The parameters such as frequency, number of spikes, amplitude and synchronization are critical for the network's operation and depend mainly on the character, strength and timing of the stimulus [22], [38]. Comparison of various neuron models can be found in [20].

II. Neuron Model

There are two major types of biologically inspired artificial neuron models, namely conductance based models such as Hodgkin–Huxley or Connor–Stephens, and the integrate-and-fire models, such as the MacGregor model. Conductance based models allow for detailed dynamics of a neuron's membrane potential and spike generation. They imitate the biological neurons' response by modeling several ion channels, like sodium, potassium, calcium, etc. Advantages of conductance models are the possibility of modeling post-inhibitory rebounds, bursting, and the multiple-compartmental structure of a single neuron. Considering the compartmental geometry of the neuron (nucleus, dendrites, and axon) increases the model's accuracy [19] but it also considerably raises the computational complexity of a model. In spite of the fact that the computational power is constantly increasing, less complex neuron models permit construction of much larger and faster computing networks. Furthermore, in many applications, such as modeling of learning processes, modeling of spike generation can be simplified (allowing for a larger time step for integration and decrease in the number of variables and formulas), thus considerably decreasing computation time [21]. The simplification decreases degree of biological similarity, but allows observation of the network from a wider perspective. The family of integrate-and-fire neuron models has a simplified spike generation mechanism while providing an accurate approximation of the membrane potential and other neuron properties like refractory properties and adaptation to stimuli. Simplification of spike generation allows for improved computation speed as compared with conductance based models. In our NSN we use the integrate-and-fire neuron model, which is based on the MacGregor model [26]. It models the biological neuron behavior closely in terms of subthreshold membrane potential, potassium channel response, refractory properties, the neuron's excitation and inhibition, and adaptation to stimuli.

Manuscript received October 20, 2004; revised February 10, 2005.

W. Swiercz is with the Department of Neurology, Health Sciences Center, University of Colorado at Denver, Denver, CO 80262 USA (e-mail: Waldemar.Swiercz@uchsc.edu).

K. Cios is with the Department of Computer Science and Engineering, Health Sciences Center, University of Colorado at Denver, Denver, CO 80217 USA (e-mail: Krys.Cios@cudenver.edu).

K. Staley is with the Department of Neurology and Pediatrics, Health Sciences Center, University of Colorado at Denver, Denver, CO 80262 USA (e-mail: Kevin.Staley@uchsc.edu).

L. Kurgan is with the Electrical and Computer Engineering Research Facility, University of Alberta, Edmonton, AB T6G 2V4, Canada (e-mail: LKurgan@ece.ualberta.ca).

F. Accurso and S. Sagel are with the Children's Hospital, Denver, CO 80218 USA (e-mail: Accurso.Frank@tchden.org; Sagel.Scott@tchden.org).

Digital Object Identifier 10.1109/TNN.2005.860834

It is described by (1) through (4).
Spike generation:

$$S = \begin{cases} 1 & E \geq T_h \\ 0 & E < T_h \end{cases}. \tag{1}$$

Refractory properties:

$$\frac{dG_K}{dt} = \frac{-G_K + B \cdot S}{T_{\mathrm{GK}}}. \tag{2}$$

Threshold Accommodation:

$$\frac{dT_h}{dt} = \frac{-(T_h - T_{h0}) + c \cdot E}{T_{\mathrm{th}}}. \tag{3}$$

Transmembrane potential: (Please see (4) shown at the bottom of the page.) where
Transmembrane potentials:

$$\mathrm{E} = \mathrm{V} - \mathrm{V_r} \quad \mathrm{E_K} = \mathrm{V_K} - \mathrm{V_r}$$
$$\mathrm{E_i} = \mathrm{V_i} - \mathrm{V_r} \quad \mathrm{E_e} = \mathrm{V_e} - \mathrm{V_r}$$

- V – membrane potential;
- $\mathrm{V_r}$ – membrane resting potential;
- $\mathrm{V_K}$ – potassium resting potential;
- $\mathrm{V_i}$ – inhibitory resting potential;
- $\mathrm{V_e}$ – excitatory resting potential.

Transmembrane conductances:

$$\mathrm{G_K} = \mathrm{g_K}/\mathrm{G}$$
$$\mathrm{G_i} = \mathrm{g_{si}}/\mathrm{G}$$
$$\mathrm{G_e} = \mathrm{g_{se}}/\mathrm{G}$$

- $\mathrm{g_K}$ – potassium resting conductance;
- $\mathrm{g_{si}}$ – inhibitory resting conductance;
- $\mathrm{g_{se}}$ – excitatory resting conductance;
- G – membrane resting conductance.

$\mathrm{SCN} = \mathrm{SC}/\mathrm{G}$ – Current through a membrane:

- SC – current injected to cell;
- $\mathrm{T_{GK}}$ – time constant for $\mathrm{G_K}$ decay;
- $\mathrm{T_h}$ – threshold value;
- $\mathrm{T_{h0}}$ – resting value of threshold;
- $\mathrm{T_{th}}$ – time constant for decay of threshold;
- $\mathrm{T_{mem}}$ – membrane time constant;
- $\mathrm{T_{mem}} = \mathrm{C/G}$;
- C – for the second training phase capacitance;
- c – determines rise of threshold $\mathrm{c} \in [0, 1]$;
- B – postfiring potassium increment;
- N – noise;
- S – flag showing neuron firing $\{0, 1\}$.

III. Neuron Signals Transmission

Properties of the neuron model we use are based on biological neurons from hippocampus, more precisely on neurons from its CA3 region. The majority of neurons within this region are excitatory (pyramidal), while the remaining neurons are inhibitory (interneurons) [35]. When a neuron fires, it generates action potentials (spikes) that depending on a particular neuron type can have excitatory or inhibitory effect on the neighboring/connected neurons. Most of the signals travel along the axon and are transmitted via synaptic connections to other neurons' dendrites by neurotransmitters. In excitatory synapses signals are carried by glutamate while in inhibitory synapses they are carried by γ-amino-butyric acid (GABA). Glutamate then activates excitatory N-methyl-D-aspartate (NMDA) (long lasting) and α -amino-3-hydroxy-5-methylisoxazole-4-propionic acid (AMPA) (rapid) ionotropic receptors, while GABA activates inhibitory $\mathrm{GABA_A}$ (fast) and $\mathrm{GABA_B}$ (slow) receptors. Receptor activation causes postsynaptic conductance changes that in turn change the neuron's membrane potential. The amount and direction of that change depend on synaptic connection strength, signal strength, and the pattern of stimulation. In the network model described here we simulate the effects of fast signal transmission (only AMPA and $\mathrm{GABA_A}$ receptors). Slow, long-lasting effects are not simulated. The synaptic connection type (excitatory or inhibitory) depends on the presynaptic neuron. The neuron cannot be both excitatory and inhibitory thus all synaptic connections originating from a particular neuron are of the same type.

The signal transmission described above is implemented in our model in the following way. The arriving spikes change the postsynaptic conductance, thus changing the membrane potential. There is a synaptic strength (weight) associated with each synaptic connection, so the weighted sum of all excitatory and the weighted sum of all inhibitory synaptic conductances are calculated (yielding excitatory and inhibitory input values). These values determine the change in the membrane potential (4). If the membrane potential reaches the threshold value, the neuron fires, generating a spike train traveling along the axon to all connected neurons (1).

Another property implemented in MacGregor's model is accommodation of the membrane threshold to the stimulating signals (3). It causes the neuron to require a stronger stimulus for the generation of consecutive spikes in the train. In addition, immediately after the spike generation the neuron is incapable of firing for a short time called absolute refractory period. Following the absolute refractory period is an interval known as the relative refractory period when the neuron can only respond to a very strong stimulation (2).

In order to mimic biological neuron behavior even closer we implemented simulation of noise for the membrane potential [14]. The used noise has a maximum range of -0.5 to 1.0 of the initial threshold value, with a normal probability distribution. Parameters of distribution are mean of 0.25 and standard deviation of 0.3. The ultimate amount of noise is calculated as a per-

$$\frac{dE}{dt} = \frac{-E + G_K \cdot (E_K - E) + G_e \cdot (E_e - E) + G_i \cdot (E_i - E) + SCN + N}{T_{\mathrm{mem}}} \tag{4}$$

centage of the membrane potential, which is one of the model's parameters. In Fig. 1 we show neuronal responses to stimulation with noise applied to the membrane potential. The upper section of images shows the neuron's membrane potential response (E, darker line), along with the corresponding changes in the threshold (Th, brighter line). The neuron fires each time a membrane potential value reaches the threshold. The middle section shows the neuron's input. For image in Fig. 1(a) the external current value, SCN, constitutes the input. In Fig. 1(b) the input is represented by the activity of the excitatory G_e (above the center line in the image in the middle) and the inhibitory G_i (below the center in the same image) conductances. The bottom section of the images illustrates activity of the potassium channel.

Initial stimulation of the network is done via clamp electrode models injecting current into selected neurons. The injected current raises the membrane potential above the threshold, causing the neurons to fire. After an initiating period, the current injections can be stopped in order to observe and record the network activity.

IV. Synaptic Activity Plasticity Rule

In our NSN model we use the Hebbian-type synaptic plasticity [15]. The adjustment of the strength of synaptic connections between neurons takes place every time the post synaptic neuron fires. If this occurs, synaptic weight values are updated according to (5). The learning rate α controls the amount of adjustment in a single iteration. It can be any positive real value; 0 means no learning. In real applications this value should not be too large since learning is a relatively slow process. To keep the synaptic connection strength within a certain range we use a sigmoidal function because synaptic connection strength cannot grow or decrease infinitely. A sigmoid works better than, say, simple boundary thresholds, since it produces a smoothly shaped learning curve.

$$w_{ij}(t+1) = \mathrm{sig}(w_{ij}(t) + \alpha_{+-} \cdot \mathrm{PSP}_{ij}(t)) \qquad (5)$$

where

- t – time;
- w_{ij} – synaptic weight between neurons i and j;
- α_{+-} – learning rate, can have different value for positive and negative adjustment;
- PSP_{ij} – postsynaptic potential value for connection between neurons i and j;
- $\mathrm{sig(x)}$ – sigmoid function.

In our previous models [9], [12], we used spike timing-dependent plasticity (STDP) [33] and temporal correlation learning (TCL) rules [10], [29], [30]. Both rules used artificial functions to evaluate the amount of synaptic strength adjustment for each synapse. The STDP formula is given in (6) and its shape illustrated in Fig. 2(a). Fig. 2(b) shows biological data on which development of the STDP is based [5]. Although both functions were developed to reflect synaptic strengths adjustments observed during biological experiments, they represent a non-physiological object in the model

$$\mathrm{STDP}(\Delta t) = \begin{cases} \alpha_+ \exp(-\Delta t/\tau_+) & \text{if } \Delta t > 0 \\ -\alpha_- \exp(\Delta t/\tau_-) & \text{if } \Delta t \le 0 \end{cases} \qquad (6)$$

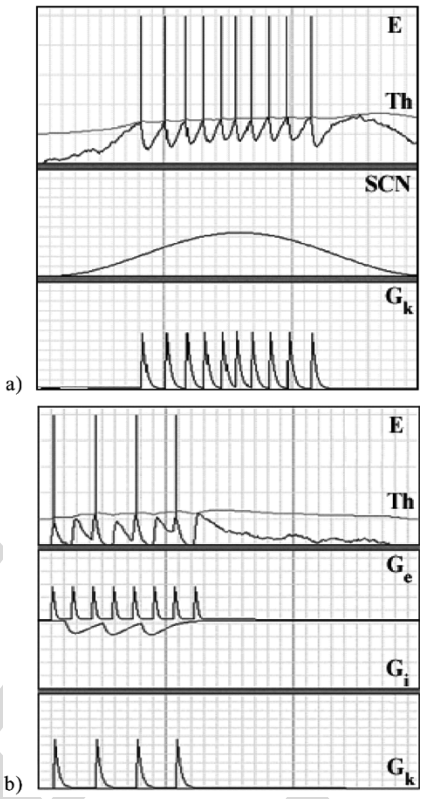

Fig. 1. Neuron responses to (a) external artificial stimulation with clamp electrode and (b) natural stimulation with excitatory and inhibitory spikes, where the E-membrane potential (darker line); Th-threshold (brighter line); G_e-excitatory conductance [above the center in the middle of b)]; G_i-inhibitory conductance [below the center in b)]; G_K-potassium channel conductance; SCN-external stimulation signal.

where

- Δt – time between pre and post synaptic neuron firings;
- α_{+-} – learning rate;
- τ_{+-} – time constant.

In contrast to these rules, our new Synaptic Activity Plasticity Rule (SAPR) uses actual synaptic dynamics to evaluate the amount of adjustment. It is interesting to note that the estimated shape of the function shown in Fig. 3(a) fits experimental data well [5], [13], see Fig. 2(b). The advantage of our approach is that instead of an artificial function we use actual value present in each synapse.

The SAPR rule is simple and agrees with Hebbian-type plasticity. Modification of the synaptic weights between pre- and postsynaptic neurons takes place every time the postsynaptic neuron fires. When this occurs all the neuron's incoming synapses are evaluated, and their synaptic strength is adjusted depending on the particular synapse type and its recent activity. The amount of adjustment is proportional to the contribution of a particular synapse to the neuron's firing.

If the particular excitatory presynaptic neuron spike arrives before the postsynaptic neuron fires, the related synapse has positive contribution, thus its synaptic strength increases by an amount proportional to the current postsynaptic potential (PSP) value. When the excitatory presynaptic neuron's spike arrives after the postsynaptic neuron fires, it has no contribution to the

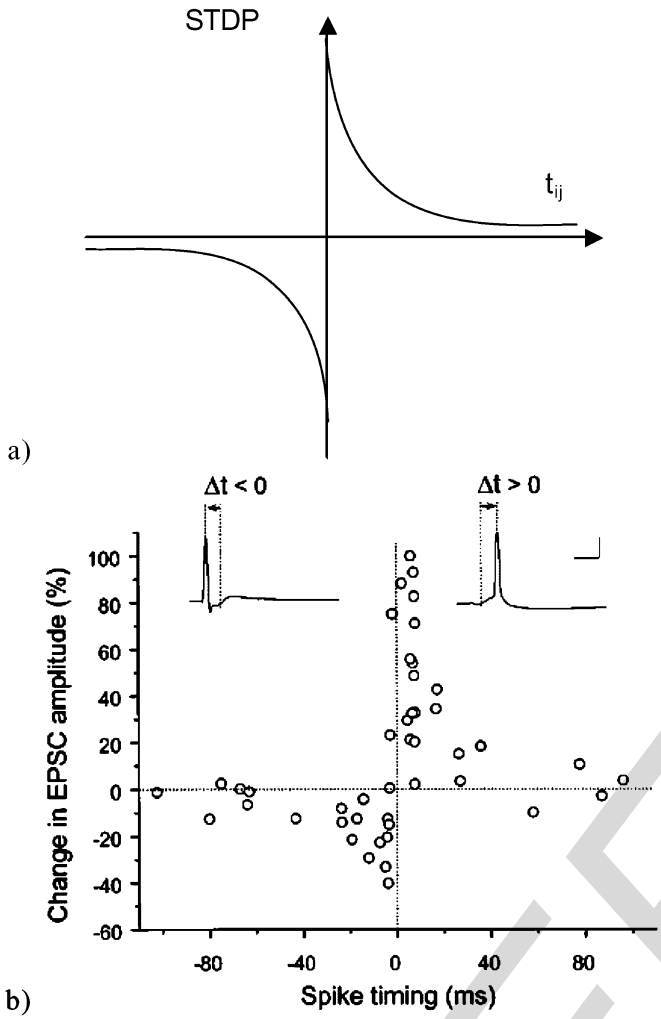

Fig. 2. a) STDP function shape and b) biological data on which STDP was based [5], [13].

recent firing. Its strength is decreased by an amount proportional to the current PSP value.

For inhibitory synapses, biological learning rules are less clear and are hard to demonstrate physiologically. Long-term potentiation (LTP) [28] and long-term depression (LTD) [8], [3] of inhibitory synapses have been reported but the literature is scant compared to that for LTP and LTD of glutamatergic synapses. We do not know if most types of GABAergic synapses are even capable of plasticity; some people think that long-term plasticity of the inhibitory system would be a bad idea [25]. Thus we included inhibitory plasticity in our model to see if it would make sense computationally. We implemented it as the reverse of the rule for excitatory synapses. The reason is that the role of the inhibitory synapse is opposite, namely, to depress the postsynaptic neuron in order to prevent it from firing.

There is no explicit equation or function shape for the synaptic strength adjustment in the SAPR. We can only approximate possible function plot by using a general PSP shape. Fig. 3(a) gives a general example of a learning function for excitatory and inhibitory synapses; the actual shape depends on the particular synapse parameters, current synaptic strength and learning rate used. It is important to note that in contrast

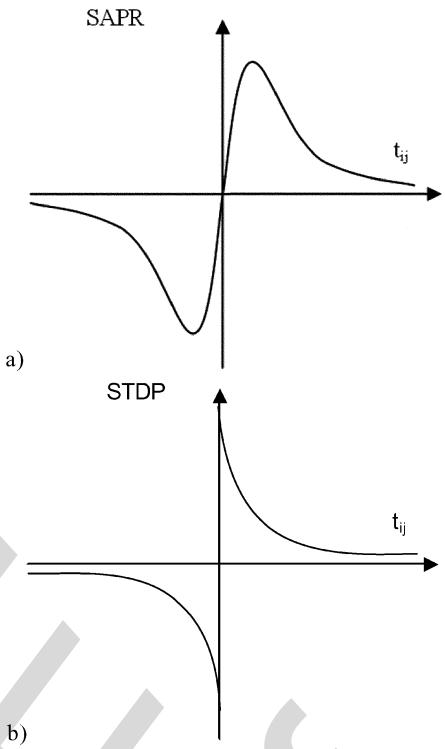

Fig. 3. Comparison of learning function shapes: (a) SAPR and (b) STDP.

to previously used STDP function [see Fig. 3(b)], the SAPR function is continuous, has an finite range of values, and its shape mimics biological observations [13].

Our plasticity hypothesis is related to findings reported in [6]. Using stochastic Spike Response Model (a variation of integrate and fire neuron model) the authors used entropy minimization to simulate neuron response. One of their results was a variation of STDP learning shape; as can be seen in Fig. 4. Although physiologically and computationally correct, the learning curve requires numerical integration that is not feasible to perform in real time within synapse. The authors hypothesize that physiologically there may be other way of computing their learning curve. They propose their SAPR plasticity as the alternative to numerical integration.

The postsynaptic potential (PSP) modification used in SAPR is a result of synaptic current alteration elicited by changes of the synaptic conduction by the arrival of the action potential to the synaptic connection. The PSP can be either increased (excitatory PSP, EPSP) or decreased (inhibitory PSP, IPSP). These changes directly affect the neuron's membrane potential. The synaptic conductance between the neurons i and j is obtained via (7). Fig. 5 shows the normalized shapes of the EPSP and IPSP.

$$g_{ij}(t) = \frac{t - \Delta t_{ij}}{T_{ij}} \cdot \exp\left(1 - \frac{t - \Delta t_{ij}}{T_{ij}}\right) \tag{7}$$

where g_{ij}—synaptic conductance; t—time; Δt_{ij}—propagation time; T_{ij}—synapse time constant.

The SAPR plasticity rule reflects both LTP and LTD. LTP and LTD are phenomena associated with learning and memory observed in biological networks [1], [34]. Many researchers

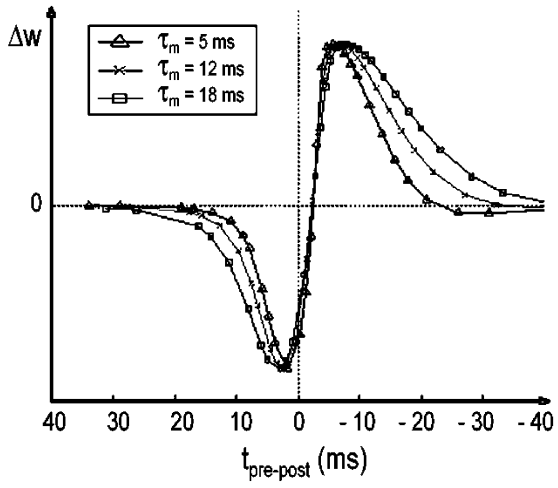

Fig. 4. STDP type learning shape resulting from neuron output entropy minimization [6]; Δw—weight adjustment, $\Delta t_{\mathrm{pre-post}}$—time between pre synaptic spike arrival and post synaptic neurons firing, τ_{m}—membrane potential time constant.

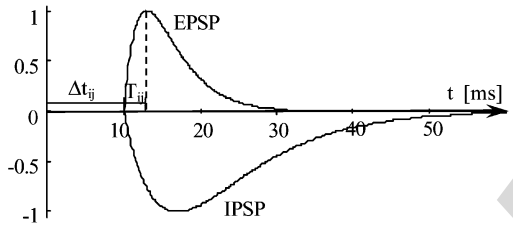

Fig. 5. EPSP and IPSP normalized shapes. Where: t—time; Δt_{ij}—propagation time; T_{ij}—synapse time constant.

consider LTP as the most important process underlying hippocampal learning [16], [38].

In order to test our synaptic plasticity rule and the NSN we used them for image processing tasks, using two different sets of data described below. The reason for testing our rule on image data is that it is easy to visually judge accuracy of results.

V. Diabetic Retinopathy Images and Preprocessing

One of the complications caused by diabetes is Diabetic Retinopathy (DR). Elevated blood sugar in diabetics causes the blood vessels in the retina to leak, close, and proliferate, damaging the retina. DR is one of the major causes of blindness. Nearly all patients with diabetes will eventually develop DR, and it is possible that they will not know that they have it until the later stages of the disease [2]. With appropriate treatment over 90% of visual loss from DR can be prevented. Thus, early diagnosis of DR is very important, which entails regular examination of diabetic patients. The detected DR can be appropriately treated, dramatically slowing down the disease progress. Unfortunately, about 50% of diabetic patients are never examined and only 30% of them are examined regularly [37]. An automatic computer analysis of retinal images that recognized DR lesions could substantially improve the efficiency of screening examinations. Only a technician would be required to do the screening, making wide-spread retinal exams and early detection of DR much more feasible. Computerized retinal image analysis may also decrease the overall costs for both patients and clinics, because only patients diagnosed positively for sight threatening DR would be required to see the ophthalmologist.

The positive diagnosis of DR is based on existence of the following lesions on the eye fundus: neovascularization, cotton wool spots, exudates, microaneurysms, and hemorrhages [24]. The severity level of the disease is diagnosed depending on the pattern of abnormalities. The digital fundus images used in our research for detection and diagnosis are 2160 pixels wide and 1140 pixels high, and have a 24 bit color depth. It is well known that the analysis of the green layer of the image can provide almost full information about DR (red and blue layers contain almost no information), so only the green layer was used in our research [9], [12].

The digital images contain some amount of noise. There are also other factors that cause difficulties in lesion detection. Image parameters such as color, contrast, and brightness are distinct for each patient. Sometimes those values are different for each eye of the same patient, or they may change between visits. Another problem for lesion detection is nonuniformity of the image background intensity. To diminish the influence of those factors the images must be filtered. For that purpose we used the following filters: the Center Weighted Median (CWM) filter to remove noise [4] and the Flat Fielding (FF) filter which is based on a Fast Fourier Transform (FFT) to make the intensity of the images more uniform [31]. The CWM filter is very effective in removing noise from the images. It works almost like the Median Filter (MF), however it has an advantage over the simple MF in that it preserves image details. After applying the filters to the image, its histogram is expanded to increase the contrast. Preprocessed images are then used as input for clustering using a network of spiking neurons.

The large dimensions of the images cause difficulties in performing the computations on the entire image using the network of spiking neurons because of high memory requirements and very long computation times. To obtain results more rapidly we decided to process sub-images with dimensions of 20×20 pixels. Despite the small size of the sub-images, we were able to assess the results of detection and validate our synaptic plasticity rule. Fig. 6 illustrates the image sample, containing part of a blood vessel and a small hemorrhage, before and after preprocessing.

VI. Cystic Fibrosis Images and Preprocessing

The Cystic fibrosis (CF) is the most common, lethal inherited disorder in the Caucasian population, now affecting approximately 30 000 people in the United States [39], [32]. It is caused by mutations in the gene encoding the cystic fibrosis transmembrane conductance regulator (CFTR) protein. Though multiple organ systems are affected in this disease, lung involvement is the primary cause of morbidity and mortality. A vicious cycle of chronic infection with CF-related pathogens (especially *Pseudomonas aeruginosa*) and excessive inflammation progressively damage the airways and lung parenchyma, resulting in widespread bronchiectasis (an abnormal dilation of the bronchi that is usually irreversible) and other structural lung abnormalities

including bronchiolectasis, stenosis, and fibrosis of small airways, cystic disease, and emphysema [23], [32]. Bronchiectasis and these other structural lung abnormalities are directly responsible for many clinical manifestations including productive cough, recurrent bronchitis, progressive obstructive airways disease, exercise intolerance, dyspnea, hemoptysis, anorexia, and weight loss. The majority of CF patients ultimately die of respiratory failure.

High-resolution computed tomography (HRCT) of the chest is a sensitive measure of early CF lung disease and has provided evidence of bronchiectasis, peribronchial wall thickening, mosaic perfusion, and mucus plugging in infants and children with CF [7], [17], [27]. It is clearly more sensitive and accurate than conventional chest radiography in delineating the extent and severity of bronchiectasis. Since airway injury and bronchiectasis are the major consequences of progressive CF lung disease, the primary computed tomography (CT) measures will be severity of airway changes (bronchial wall thickness, bronchial lumenal diameter), and extent of bronchiectasis (number and location of bronchiectatic airways).

HRCT images provide axial slices of a patient's lungs with a resolution of 512×512 pixels. Since the images are computer generated, they do not require much preprocessing [36]. The only filtering we apply is CWM filter to get rid of salt-and-pepper noise. Fig. 7 illustrates a few airways in the same HRCT image from a patient with CF before and after preprocessing.

VII. Network Topology

As mentioned earlier we based the properties of our network on the CA3 hippocampal region. There exist uncertainty about the estimated number of pyramidal cells and interneurons in hippocampus. In order to build a network model we used the ratios reported in [38], where the authors estimate that about 90% of neurons in the region are pyramidal, and the remaining 10% are interneurons. Pyramidal cells can connect to neurons in other regions. Some of these connections can be distant, with conduction delays over 20 ms. Pyramidal cells can also create recurrent connections to other pyramidal cells within the same region and local connections to interneurons [35]. The ratio of recurrent vs. interneuron connections is about 5:1. Interneurons connect locally to neighboring pyramidal cells. Inhibitory connections are short but dense; they are also reliable and have almost no delay. Although there are reports of interneurons connecting to other interneurons (less than 10% of inhibitory connections), we did not implement them within our NSN model.

In our previous research [12] we used a similar network of spiking neurons for image clustering [9]. The network used the Temporal Correlation Learning rule [10], [11], [29], and was shown capable of unsupervised clustering of the data [30] without a priori specifying the number of clusters. However, because of the long processing time and memory requirements we decided to change the network structure and method of neuron stimulation, which required development of the new plasticity rule.

The new network topology is shown in Fig. 8. The new network consists of two layers of excitatory neurons and one layer of inhibitory neurons.

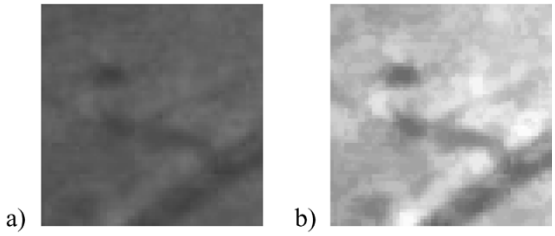

Fig. 6.DR image preprocessing: (a) original image and (b) result.

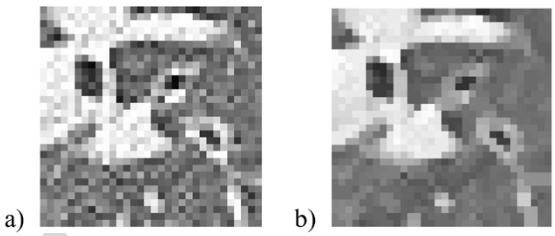

Fig. 7. CF image preprocessing: (a) original image and (b) result.

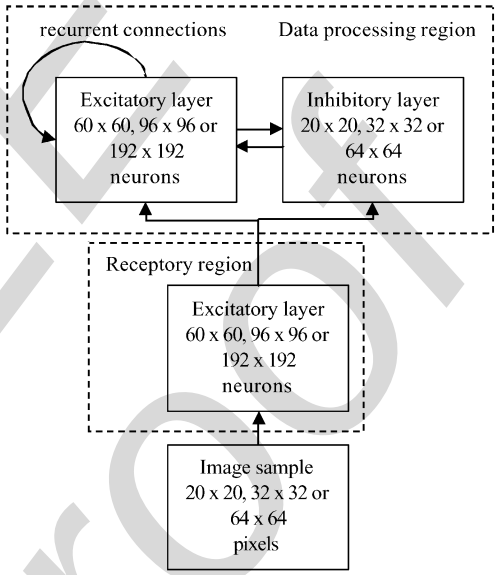

Fig. 8. Network topology.

Neurons characterized by the same parameters and functions are grouped into layers. The first excitatory layer represents the receptive/sensory region of the network. The second excitatory layer together with inhibitory layer represents data processing region. The dimensions of the receptive region layer are three times the size of the processed image to take care of receptive fields overlapping. The dimensions of the data processing excitatory layer are also three times bigger than the image. Dimensions of the inhibitory layer are the same as the dimensions of the image to keep the excitatory to inhibitory ratio of 9:1 [38]. The synaptic connections between the neurons are organized as follows. The receptive region layer has only outgoing connections to the data processing region's excitatory and inhibitory layers. Connections span from each neuron within the receptive region layer to the corresponding neuron within the data processing excitatory layer. For inhibitory neurons stimulation, each neuron within a 3×3 receptive area is connected to a single inhibitory neuron in the data processing region. In the

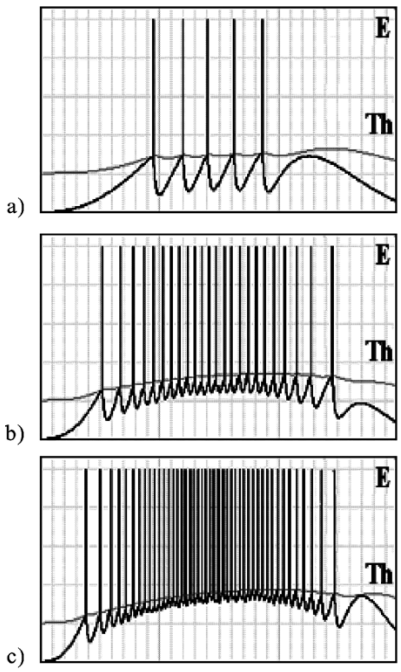

Fig. 9. Neuron's response to artificial external clamp stimulation with input sinusoid shape and amplitude of (a) 15, (b) 50, (c) 100; noise was not applied. Darker line represents the membrane potential, where as the brighter line represents the threshold level.

data processing layer, synaptic connections span from excitatory to inhibitory neurons and from inhibitory to excitatory neurons. Additionally there are recurrent connections between the layers' excitatory neurons. Each excitatory neuron within the 3×3 area in the data processing layer is connected to the corresponding inhibitory neuron. The outputs of the inhibitory neuron are connected back to the nine excitatory neurons. For the recurrent connections, each neuron of the excitatory layer is connected to the eight neighboring excitatory neurons. The initial strengths of synaptic connections coming out of the receptive layer are set to the maximum value to assure that the original stimulation is delivered to the following layers. All remaining synaptic connections' strengths are set to random values between values 0.6 and 1.6. The minimum connection strength is 0.1 and maximum is 2.5.

VIII. Network Stimulation

The input to the network is organized as follows. The neurons within the receptive layer are stimulated with current clamp electrodes. Each clamp represents a single pixel of the image. The amplitude of stimulation strength applied by the clamp is equal to normalized image pixel intensity. The stimulation function shape is a positive-valued sinusoid with a period of 300 ms. We use a sinusoidal function instead of a transient step input because it is a more natural way of stimulation. It does not add any additional computational complexity since the function is stored within the lookup table.

The results of the stimulation in the model can be related to the results of light stimulating green cones within the retina (green because we apply a green image layer for computations).

The neurons' response to the stimulation is nonlinear with maximum sensitivity in the middle range. Neuronal nonlinearity has been discussed in the literature, e.g., [13], [22], and has its equivalent in biology, e.g., in human vision. The best vision, translating to best distinction between colors, shades or objects occurs in so-called average lightning conditions, while too bright or too dark lightning conditions make it hard or impossible do distinguish objects. Fig. 9 shows examples of a single neuron responses to stimulations of various amplitudes. The stimulation signal shape is a sinusoid. The strength of the neuron's response, i.e., the membrane potential E (shown as darker line in Fig. 9) is proportional to the stimulation signal amplitude. Every time the neuron membrane potential E reaches the threshold Th (shown as brighter line) the neuron generates action potential.

TABLE I
Original Diabetic Retinopathy Image Samples

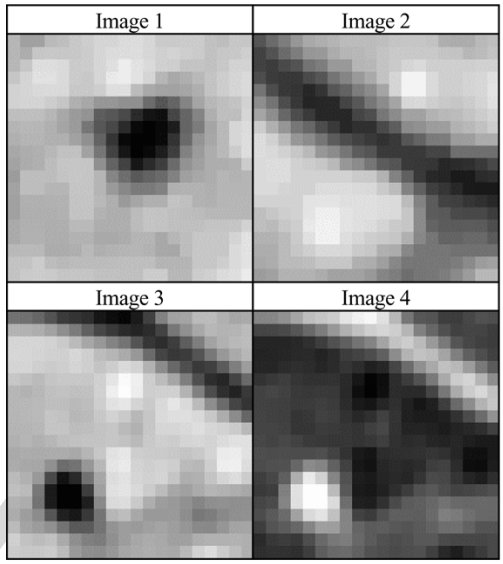

IX. Experiments

We performed a series of experiments on various DR and CF images with resolutions of 20×20 pixels and 32×32 pixels, respectively, using the NSN. The α_+ and α_- parameters for synaptic plasticity are changed in each series. Network topology, properties of the neurons and synaptic connections used in the experiments, along with initialization of connection weights are described above. For majority of the experiments the network had the total of 7600 (for 20×20 pixels images) and 19 456 (for 32×32 pixels images) neurons. Each experiment was simulated over 300 ms time interval. Images were preprocessed, as described earlier, and then presented to the network. Current clamp amplitudes were set to the values equal to the normalized intensities of image pixels. At the end of each stimulation, the strengths of synaptic connections were saved for analysis. More precisely we stored the strengths of all recurrent excitatory synaptic connections, and the strengths of all inhibitory to excitatory synaptic connections.

In order to check if the initial weights have influence on the results, we repeated each experiment with different random initial weights. As expected, no influence was found since differences between the results were marginal.

TABLE II
RESULTS OF SIMULATION FOR ALL LEARNING RATES $\alpha_+ = \alpha_- = 1$

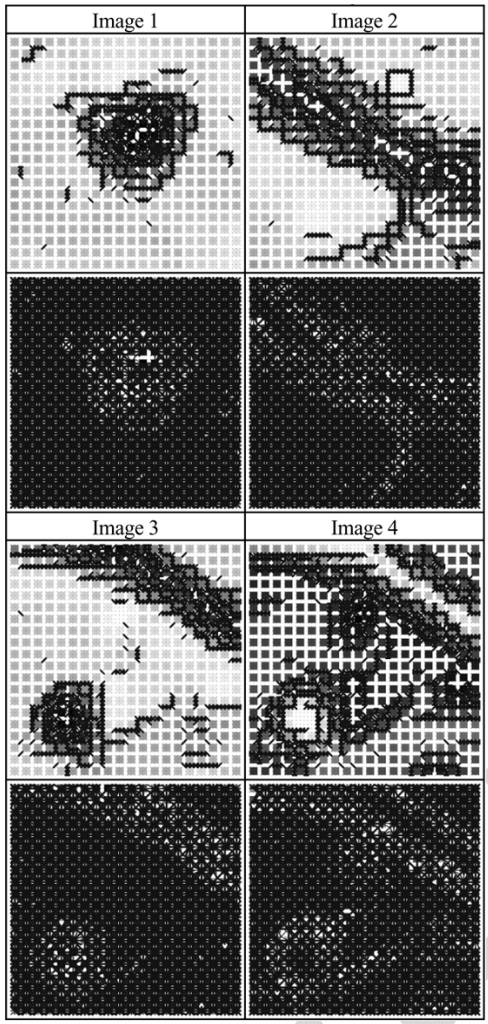

TABLE III
RESULTS OF SIMULATION FOR BOTH EXCITATORY AND INHIBITORY LEARNING RATES $\alpha_+ = 0.6$ AND $\alpha_- = 0.8$

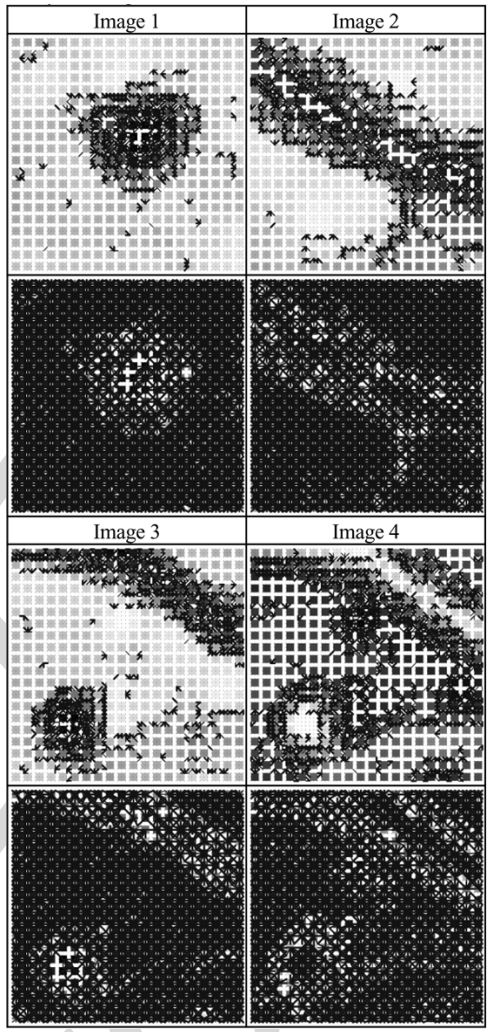

Another series of experiments were performed to observe how the network performs without inhibitory learning. The experiments were performed in the same manner as described in the previous section, except inhibitory learning was blocked. Weights of inhibitory connections were set to random values and did not change through whole experiment (parameters α_+ and α_- were set to 0.01).

We also repeated the above experiments with inhibition completely blocked. We were interested to see how the model performed in this extreme case.

Finally, in order to test how the network performs for larger data we applied it to image samples with a resolution of 64×64 pixels. Additionally, this time the images were not preprocessed. The higher resolution increased the number of neurons within the network to 147 456 and the simulation time average to over three minutes. Comparing it to the experiment with 20×20 pixels images, the number of pixels increased about 10 times, the number of neurons increased 20 times, and the average computation time increased about 10 times.

X. RESULTS

To analyze the results of our computations we defined the threshold separating strong connections from the weak ones. Very weak connections should be considerably depressed, resulting in poor and undependable signal transmission [38]. As described earlier the connections in our model take values from 0.1 (very weak) to 2.5 (very strong). We set the threshold value to 0.8, which is about $1/3$ of the maximum connection value in order to differentiate strong (surviving) connections from weak ones.

Table I shows original DR images and Tables II through IV the results of experiments with various learning rate settings.

The first and third rows in Tables II through IV show excitatory recurrent synaptic connections and the second and fourth row shows the inhibitory to excitatory synaptic connections, where each small square on the resulting images represents a 3×3 receptive area of excitatory neurons corresponding to one image pixel and its intensity value, and dark lines show strong synaptic connections that remained after stimulation.

Surviving excitatory recurrent synaptic connections concentrate along well defined edges of objects, separating areas of

TABLE IV
RESULTS OF SIMULATION FOR LEARNING RATES: EXCITATORY $\alpha_+ = 0.5$ AND $\alpha_- = 0.7$, AND INHIBITORY $\alpha_+ = 0.5$ AND $\alpha_- = 0.9$

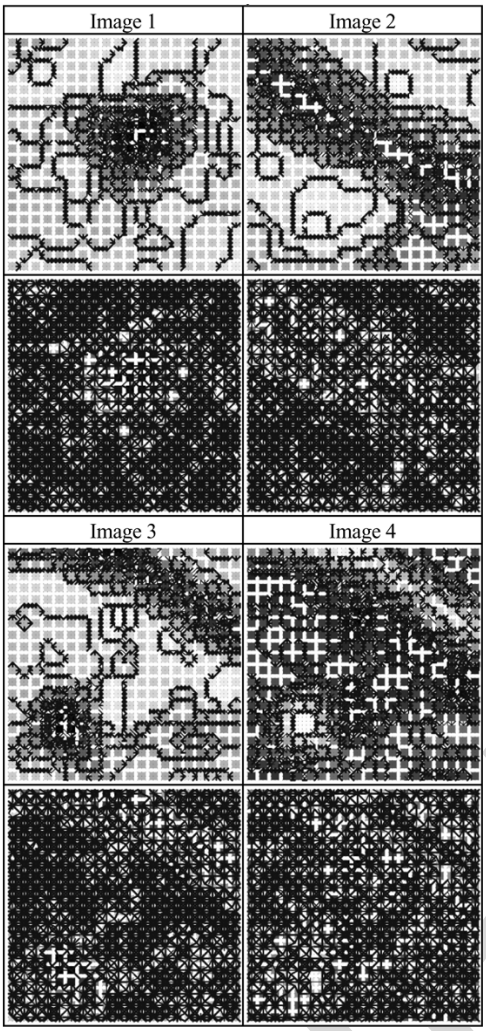

different image intensity. However for some objects it seemed as they were completely covered with surviving connections. In order to investigate this phenomenon we performed experiments on the negatives of the image samples. The example result is shown in the "Image 4" in Tables I through VI. It shows that dark areas are not covered by surviving connections but the edge thickness depends on the difference in intensity between separated areas causing small dark areas look as they were completely covered.

For inhibitory connections it is easy to notice that much more of them survive with rather high values of synaptic strengths, as compared to recurrent excitatory connections. This is consistent with the fact that in biological networks inhibitory synapses are denser and more reliable than excitatory ones. It also can be seen in our results that inhibitory connections produce, in some proportion, inverse results to recurrent excitatory synapses. They are not exact inversion because as we said earlier, inhibitory synapses are naturally stronger [18]. Excitatory to inhibitory synaptic connections are not shown because the inhibitory layer is smaller than the excitatory one, so it would be hard to correlate neurons and connections to image pixels and the rest of the results.

TABLE V
RESULTS OF SIMULATION FOR THE NETWARK WITH NO INHIBITORY LEARNING ($\alpha_+ = \alpha_- = 0.01$) AND EXCITATORY LEARNING RATES $\alpha_+ = \alpha_- = 1.0$

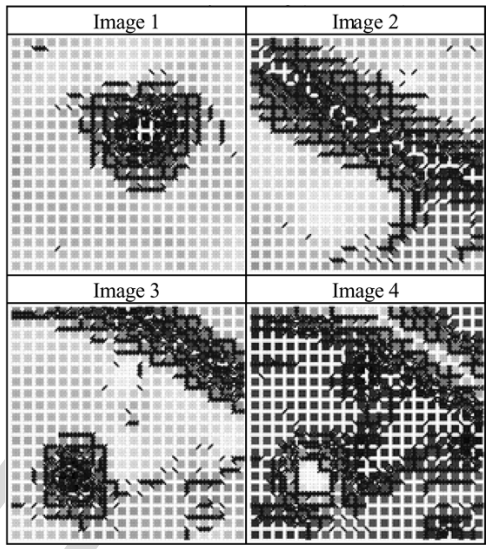

Various settings of learning rates influence the results. We initially set all learning rates $\alpha = 1$. The reason was that it directly applied synaptic weights as synaptic plasticity modifications. As can be seen, comparing Tables II and III, the results of using raw synaptic weights are very good. In spite of good results for the basic setting we also investigated a number of other settings to see what influence they may have on the NSN.

We varied the learning rate values from 0.1 to 3.0, first applying the same, then different values for excitatory and inhibitory learning rates, $\alpha+$ and $\alpha-$. The majority of settings we tested generated good results; about half of them did not differ essentially from the initial results. However there was a large group of settings that caused the network to fail. For some settings the results were similar to basic results (Table III), while for other network detected more edges, between less diverse regions (Table IV).

In the next series of experiments the inhibitory learning was completely disabled. Some results are shown in Table V (see also Table X). The results from Table V should be compared to the results of experiments with inhibitory learning enabled, shown in Table II, since the used excitatory learning rates values were the same. There is no essential difference between the results; however, with inhibitory learning (Table II) the edges are a little better defined and less noisy (see Table X). This may indicate that the inhibitory learning is not a crucial process, and that the correct outcome can be achieved without it. On the other hand, inhibitory learning possibly enables a more detailed tuning of the network.

Another series of experiments were performed with disabled inhibition (the inhibitory layer was removed). Some results are shown in Table VI. The effects of learning are poor, although the detected edges are still observable. The conclusion is that the network was strongly impaired by disabling inhibition.

In Table VII, we show the results of our old network [9], [12], for the same image samples to allow for comparison. The old results appear different from the new ones because our previous network design allowed for object clustering not edge detection.

We also applied the new NSN to the CF images to test how it performs on different kind of images. The difference between the images is that DR images are taken with a digital camera where as the CF images are generated CT scans. For CF images we used the same network topology, and settings similar to those described for DR images. Table VIII shows the results. The first row shows original image samples, the second shows recurrent excitatory connections, and the third row shows inhibitory connections to excitatory neurons. The NSN correctly detected edges in the images.

Since setting all learning rates to 1 seems to generate good results, we used it for processing of the 64×64 image samples, to test how our new network topology, stimulation and synaptic plasticity scales to bigger data. The results are shown in Tables IX and X. Again, the NSN correctly detected the edges of objects in the image with noticeably better efficiency than our previous model [9], [12] (the average computation time was about 60 times shorter). Table X compares the results of network computations with plasticity employing both excitatory and inhibitory learning vs. the results with plasticity employing only excitatory synapses learning. As seen previously in Tables II and V there is no essential difference between the results but again with inhibitory learning the edges are a little better defined and less noisy.

We stress again that the main purpose of the research was to develop and validate a biologically-inspired learning rule for use within a network of spiking neurons. Application to image edge detection problem was done because of easiness of visualizing the results. We did not intend to compete with other more efficient but loosely biologically-based, artificial neural networks and other well-established image processing methods.

XI. Conclusion

In this paper we introduced new biologically-inspired Synaptic Activity Plasticity Rule, or SAPR. The rule is simple and uses efficient plasticity mechanism with characteristics highly agreeing with experimental biological data [5], [6]. To validate the SAPR we implemented it in a network of integrate-and-fire spiking neurons (NSN) and used the network for the task of autonomous (no user input) image segmentation on two different sets of medical image data. In our previous research [9] we used a network of spiking neurons for object recognition but using a different learning rule, called Temporal Correlation [12], and were also able to obtain acceptable results. However, the computational complexity of the previous model was rather high, and thus called for improvements in network topology and its learning ability. Another reason for modification was the fact that our previous model and stimulation mechanism were rather loosely related to biological data.

The developed new simple learning mechanism, the SAPR, uses existing raw postsynaptic potential to assess the amount of synaptic weight correction during training, instead of using an artificially defined function. The SAPR, used within the NSN, was able to automatically detect edges between different regions on medical images without any supervision. The detected edges were defined by the surviving synapses, where as the thickness of the edges reflected intensity difference between two adjacent areas.

We also investigated importance of inhibition and inhibitory learning in the network. After several experiments it became obvious that inhibitory neurons and synapses are crucial for proper learning. Lack of inhibition causes strong impairment and almost completely eliminates the ability of the network to learn. Although the inhibition is crucial for learning, the synaptic plasticity of inhibitory connections was found to be nonessential, except for being a network tuning mechanism. The tuning aspect

TABLE VI
Results of Simulation for the Network With Blocked Inhibition, Excitatory Learning Rates $\alpha_+ = \alpha_- = 1.0$

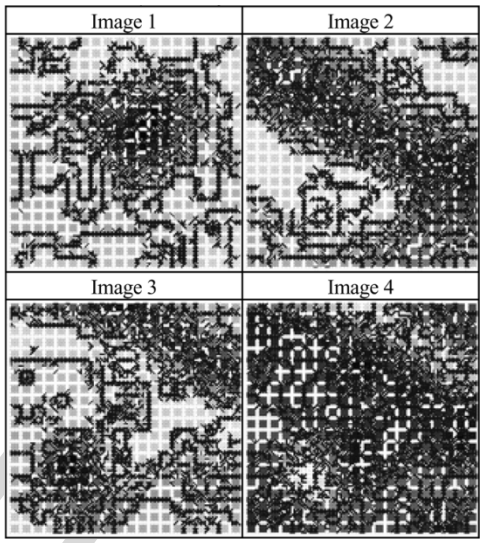

TABLE VII
Results of Clustering From Previous Research.

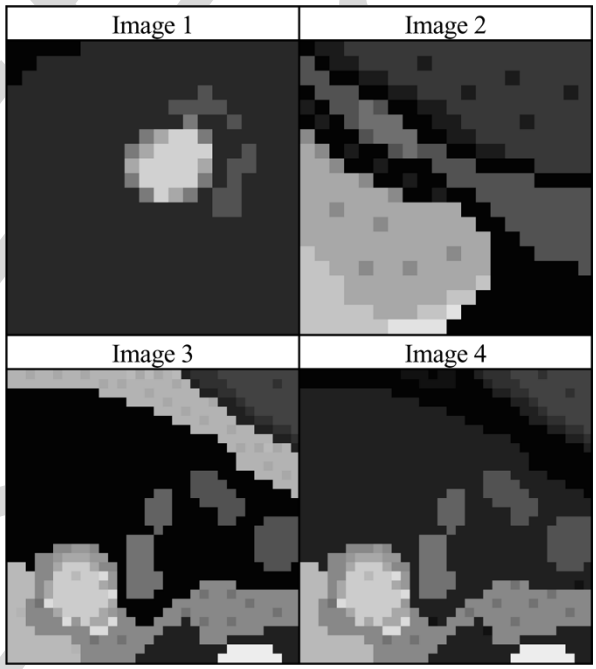

TABLE VIII
RESULTS OF SIMULATION WITH CYSTIC FIBROSIS IMAGES. EXCITATORY LEARNING RATES $\alpha_+ = 1.0$ AND $\alpha_- = 1.0$; INHIBITORY LEARNING RATES $\alpha_+ = 1.0$ AND $\alpha_- = 1.0$

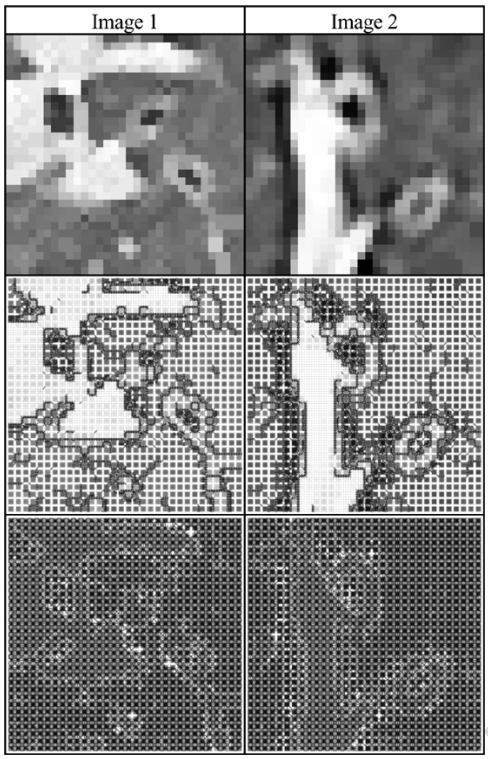

TABLE IX
RESULTS FOR 64 × 64 IMAGES SAMPLES

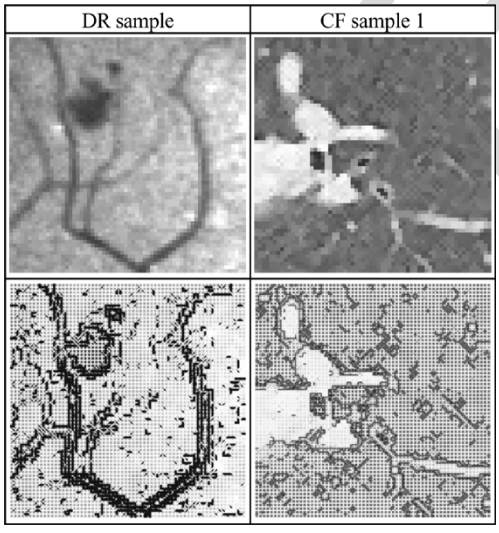

of the inhibitory plasticity was more obvious in our previous work (it caused significant improvement of the results [9], [12]) but with SAPR importance of inhibitory learning was reduced.

The developed SAPR plasticity rule was validated, within the network of spiking neurons, via using it for automatic edge finding in medical images. In addition, the biological correctness of the model was improved in terms of topology, stimulation and signal propagation. All these modifications increased model efficiency; the time required to process a single image decreased by about 60 times and the required memory space was decreased by over 50% when compared with [12].

TABLE X
COMPARISON OF 64 × 64 NSN RESULTS FOR FULL SYNAPTIC PLASTICITY AND FOR DISABLED INHIBITORY LEARNING

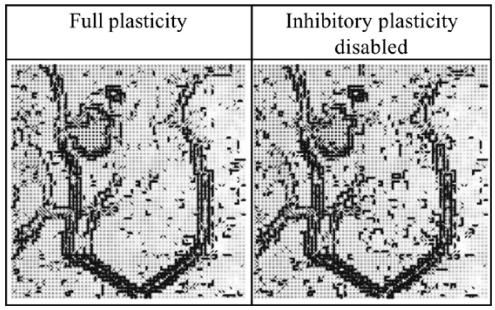

In the future we plan to use our NSN model with the SAPR to model spontaneous activity in the hippocampal CA3 neural network. The new model will allow us to test specific hypotheses regarding the nature of real neural network activity, such as the idea that bursts of spontaneous activity are limited by the supply of releasable neurotransmitter at synaptic connection between neurons in the network. Area CA3 is a well-studied model of epileptic activity, and we hope that our NSN model will provide new insights into the origin and termination of seizure activity.

REFERENCES

[1] L. F. Abbot and S. B. Nelson, "Synaptic Plasticity: Taming the beast," *Nature Neurosci. Suppl.*, vol. 3, pp. 1178–1183, 2000.
[2] L. P. Aiello *et al.*, "Diabetic retinopathy," *Diabetes Care*, vol. 21, no. 1, pp. 143–156, 1998.
[3] J. S. Bains, J. M. Longacher, and K. Staley, "Reciprocal Interactions between CA3 network activity and strength of recurrent collateral synapses," *Nature Neurosci.*, vol. 2, no. 8, pp. 720–726, 1999.
[4] Image and video processing, in Academic Press, A. Bovik, Ed., 2000.
[5] G. Bi and M. Poo, "Synaptic modifications in cultured hippocampal neurons: Dependence on spike timing, synaptic strength, and postsynaptic cell type," *J. Neurosci.*, vol. 18, no. 24, pp. 10 464–10 472, 1998.
[6] S. Bohte and M. C. Mozer, "Reducing spike train variability: A computational theory of spike-timing dependent plasticity," in *Adv. Neural Inf. Processing Syst.*, L. K. Saul, Y. Weiss, and L. Bottou, Eds. Cambridge, MA: MIT Press, 2005, vol. 17, pp. 201–208.
[7] A. S. Brody, P. L. Molina, J. S. Klein, B. S. Rothman, M. Ramagopal, and D. R. Swartz, "High-resolution computed tomography of the chest in children with cystic fibrosis: Support for use as an outcome surrogate," *Pediatr. Radiol.*, vol. 29, pp. 731–735, 1999.
[8] E. H. Chang, V. C Kotak, and D. H. Sanes, "Long-term depression of synaptic inhibition is expressed postsynaptically in the developing auditory system," *J. Neurophysiol.*, vol. 90, pp. 1479–1488, 2003.
[9] K. J. Cios, W. Jackson, W. Swiercz, and L. Springhetti, "Spiking neurons in clustering of diabetic retinopathy data," in *Proc. 2nd Int. Conf. Hybrid Intelligent Systems*, Santiago, Chile, 2000.
[10] K. J. Cios and D. M. Sala, "Advances in applications of spiking neuron networks," in *Proc. SPIE AeroScience 14th International Symposium, Applications and Science of Computational Intelligence III*, Orlando, FL, 2000, pp. 324–336.
[11] ——, "Networks of spiking neurons in data mining," in *Pattern Recognition: From Classical to Modern Approaches*, S. K. Pal and A. Pal, Eds: World Scientific, 2001, pp. 329–346.
[12] K. J. Cios, W. Swiercz, and W. Jackson, "Networks of spiking neurons in modeling and problem solving," *Neurocomputing*, vol. 61, pp. 99–119, 2004.
[13] P. Dayan and L. F. Abbot, *Theoretical Neuroscience*. Cambridge, MA: The MIT Press, 2001.
[14] *The Handbook of Brain Theory and Neural Networks*, 2nd ed., W. Gerstner, Ed., Cambridge, MA, 2002. Integrate and Fire Neurons and Networks.

[15] W. Gerstner and W. Kistler, "Mathematical formulations of hebbian learning," *Biol. Cybern.*, vol. 87, no. 56, pp. 404–415, 2002.
[16] M. A. Gluck and C. E. Myers, *Gateway to Memory*: MIT Press, 2001.
[17] T. H. Helbich *et al.*, "Cystic fibrosis: CT assessment of lung involvement in children and adults," *Radiology*, vol. 213, pp. 537–544, 1999.
[18] A. Horzyk and R. Tadeusiewicz, "Self-optimizing neural network," in *Advances in Neural Networks—ISNN 2004*, F. Yin, J. Wang, and C. Guo, Eds. Berlin, Germany: Springer-Verlag, 2004, pt. I, pp. 150–155.
[19] . [Online]. Available: http://neuron.duke.edu
[20] E. M. Izhikevich, "Which model to use for cortical spiking neurons?," *IEEE Trans. Neural Netw.*, vol. 15, no. 5, pp. 1063–1070, 2004.
[21] S. Jo, J. Yin, and Z. Mao, "Random neural networks with state-dependent firing neurons," *IEEE Trans. Neural Netw.*, vol. 16, no. 4, pp. 980–983, 2005.
[22] E. R. Kandel *et al.*, *Principles of Neural Science*: McGraw-Hill Companies, 2000.
[23] M. W. Konstan and M. Berger, "Current understanding of the inflammatory process in cystic fibrosis: Onset and etiology," *Pediatr. Pulmonol.*, vol. 24, pp. 137–142, 1997.
[24] G. Luo *et al.*, "Abnormality detection in automated mass screening system of diabetic retinopathy," in *Proc. 14th IEEE Symposium Computer-Based Medical System*, 2001, pp. 132–137.
[25] C. J. McBain, T. F. Freund, and I. Mody, "Glutamatergic synapses onto hippocampal interneurons: Precision timing without lasting plasticity," *Trends Neurosci.*, vol. 22, no. 5, pp. 228–35, May 1999.
[26] R. J. MacGregor, *Theoretical Mechanics of Biological Neural Networks*. New York: Academic, 1993.
[27] J. M. Marchant, J. P. Masel, F. L. Dickinson, I. B. Masters, and A. B. Chang, "Application of chest high-resolution computer tomography in young children with cystic fibrosis," *Pediatr. Pulmonol.*, vol. 31, pp. 24–29, 2001.
[28] Y. Oda, K. Kawasaki, M. Morita, H. Korn, and H. Matsui, "Inhibitory long-term potentiation underlies auditory conditioning of goldfish escape behavior," *Nature*, vol. 394, no. 6689, pp. 182–185, 1998.
[29] D. M. Sala and K. J. Cios, "Self-organization in networks of spiking neurons," *Australian J. Intell. Inf. Processing Syst.*, vol. 5, no. 3, pp. 161–170, 1998.
[30] ——, "Solving graph algorithms with networks of spiking neurons," *IEEE Trans. Neural Netw.*, vol. 10, no. 4, pp. 953–957, 1999.
[31] M. Seul *et al.*, *Practical Algorithms for Image Analysis*. Cambridge, U.K.: Cambridge University Press, 2000.
[32] R. E. Sobonya and L. M. Taussig, "Quantitative aspects of lung pathology in cystic fibrosis," *Amer. Rev. Respir. Dis.*, vol. 134, pp. 290–295, 1986.
[33] S. Song and L. F. Abbot, "Cortical development and remapping through spike timing-dependent plasticity," *Neuron*, vol. 32, pp. 339–350, 2001.
[34] S. Song, K. D. Miller, and L. F. Abbot, "Competitive hebbian learning through spike timing-dependent synaptic plasticity," *Nature Neurosci.*, vol. 3, no. 9, pp. 919–926, 2000.
[35] K. Staley, M. Longacher, J. S. Bains, and A. Yee, "Presynaptic modulation of CA3 network activity," *Nature Neurosci.*, vol. 1, no. 3, pp. 201–209, 1998.
[36] R. Tadeusiewicz and M. R. Ogiela, *Medical Image Understanding Technology*. Berlin, Germany: Springer-Verlag, 2004.
[37] H. R. Taylor, "Diabetic retinopathy: A public health challenge," *Amer. J. Ophthalmol.*, vol. 123, no. 4, pp. 545–545, 1997.
[38] R. D. Traub and R. Miles, *Neuronal Networks of the Hippocampus*. Cambridge, U.K.: Cambridge University Press, 1991.
[39] M. J. Welsh, B. W. Ramsey, F. J. Accurso, and G. R. Cutting, "Cystic fibrosis," in *The Metabolic and Molecular Bases of Inherited Disease*, C. R. Scriver, A. L. Beaudet, D. Valle, and W. S. Sly, Eds. New York: McGraw-Hill, 2001, pp. 521–588.
[40] L. Zhao, A. C. de Carvalho, and Z. Li, "Pixel clustering by adaptive pixel moving and chaotic synchronization," *IEEE Trans. Neural Netw.*, vol. 15, no. 5, pp. 1176–1185, 2004.

Waldemar Swiercz received the M.Sc. degree in automation and robotics from The AGH University of Science and Technology, Kraków, Poland, in 1999, and the Ph.D. degree in computer science from The University of Colorado at Boulder, in 2005.

He is currently a Post-Doctoral Fellow at the The University of Colorado at Denver and Health Sciences Center and Researcher at The Children's Hospital, Denver, CO. His research interests include modeling of spontaneous bursts with artificial neural networks of spiking neurons and image analysis of air trapping and airways thickening on CT scans of lungs affected by cystic fibrosis.

Dr. Swiercz is a member of the Society for Neuroscience.

Krzysztof Cios (SM'XX) **AU:PLEASE PROVIDE YEAR OF MEMBERSHIP** received the M.S. and the Ph.D. degrees from the AGH University of Science and Technology, Kraków, Poland, the MBA degree from the University of Toledo, OH, and the D.Sc. degree from the Polish Academy of Sciences, Warsaw, Poland.

He is currently a Professor at the University of Colorado at Denver and Health Sciences Center, and Associate Director of the University of Colorado Bioenergetics Institute. He also directs Data Mining and Bioinformatics Laboratory. He is a well-known researcher in the areas of machine learning, biomedical informatics and data mining. NASA, NSF, American Heart Association, Ohio Aerospace Institute, NATO, Colorado Institute of Technology, US Air Force, NIH, and Microsoft have funded his research. He published two books, over 50 journal articles, 12 book chapters, and about 70 peer-reviewed conference papers. He serves on editorial boards of *Neurocomputing*, I*EEE Engineering in Medicine and Biology Magazine*, *International Journal of Computational Intelligence*, and *Integrative Neuroscience*. He edited four special issues of journals. He serves as the Chair of the Computational Intelligence Society Chapter in the IEEE Denver section.

Dr. Cios has been the recipient of the Norbert Wiener Outstanding Paper Award, the Neurocomputing Best Paper Award, the University of Toledo Outstanding Faculty Research Award, and the Fulbright Senior Scholar Award. He is a senior member of the ACM, AAAI, Sigma Xi, and PIASA. Dr. Cios was elected a Foreign Member, Polish Academy of Arts and Sciences.

Kevin Staley received the B.S. degree in physics from The Loyola Marymount University, Los Angeles, CA, in 1979, and the M.D. degree from The University of California, San Diego, CA, in 1984.

He is currently a Professor at Pediatrics and Neurology Department, The University of Colorado at Denver and Health Sciences Center and the Director of The Staley Lab at The University of Colorado at Denver and Health Sciences Center. His research interests include synaptic physiology and network properties of CA3 hippocampal area, spontaneous network activation in epileptic seizures, and neuronal ion transport.

Lukasz Kurgan (M'XX) **AU: PLEASE PROVIDE YEAR OF MEMBERSHIP** received the M.Sc. degree with honors (recognized by an Outstanding Student Award) in automation and robotics from the AGH University of Science and Technology, Kraków, Poland, in 1999, and the Ph.D. degree in computer science from the University of Colorado at Boulder, in 2003.

He is currently an Assistant Professor in the Department of Electrical and Computer Engineering, University of Alberta, Edmonton, AB, Canada. His research interests include data mining and knowledge discovery, machine learning, computational biology and bioinformatics. He authored and co-authored several inductive machine learning and data mining algorithms and works on problems related to prediction and analysis of protein structure. He serves as an Associate Editor of the *Neurocomputing* journal.

Dr. Kurgan is a member of a steering committee of the *International Conference on Machine Learning and Applications*, and has been a member numerous conference program committees in the area of data mining, machine learning and computational intelligence. He is a member of the ACM and ISCB.

Frank Accurso received the B.S. degree in physics from The City College of New York, NY in 1968, and the M.D. degree from The Albert Einstein College of Medicine, NY in 1974.

He is currently a Professor of Pediatrics, Head of Pediatric Pulmonology, and Professor of Preventive Medicine at The University of Colorado at Denver and Health Sciences Center, and Medical Director of NCRR Pediatric GCRC Core laboratory. His research interests include noninvasive biomarkers of proteolytic activity in CF, protein expression analysis in CF, modifiers of early pancreatic injury in CF.

Dr. Accurso was awarded the Outstanding Research Mentor Award, Outstanding Clinical Faculty Award, Paul Di Sant' Agnese Award for Scientific Achievement in CF, Doris Tulcin Award for Research in CF.

Scott Sagel received the B.S. degree with honors in economics from The University of Michigan, Ann Arbor, in 1992, and the M.D. degree from The Washington University School of Medicine, St. Louis, MO, in 1996.

He is currently an Assistant Professor of Pediatrics at The University of Colorado at Denver and Health Sciences Center and the Associate Director of the Mike McMorris Cystic Fibrosis Center in Denver and the Chair of the Induced Sputum Committee for the Cystic Fibrosis Foundation's Therapeutics Development Network. His research interests include noninvasive assessments and biomarkers of lung injury in children with CF and primary ciliary dyskinesia.

Dr. Sagel is a member of the American Academy of Pediatrics and American Thoracic Society.